Chemical Engineering Journal 231 (2013) 345–354

Contents lists available at ScienceDirect

Chemical Engineering Journal

journal homepage: www.elsevier.com/locate/cej

Ultrasound assisted synthesis of calcium zinc phosphate pigment and its application in nanocontainer for active anticorrosion coatings

B.A. Bhanvase [a], Y. Kutbuddin [a], R.N. Borse [a], N.R. Selokar [a], D.V. Pinjari [b], P.R. Gogate [b], S.H. Sonawane [c,*], A.B. Pandit [b]

[a] Vishwakarma Institute of Technology, 666, Upper Indira Nagar, Pune 411 037, India
[b] Chemical Engineering Department, Institute of Chemical Technology, N.P. Marg, Matunga, Mumbai 400 019, India
[c] Department of Chemical Engineering, National Institute of Technology, Warangal, AP 506 004, India

HIGHLIGHTS

- Ultrasound assisted synthesis of calcium zinc phosphate nano pigment demonstrated.
- LbL assembly of calcium zinc phosphate nanocontainers have been achieved.
- Improvement in the anticorrosion properties of coatings due to the nanocontainers.

ARTICLE INFO

Article history:
Received 22 December 2012
Received in revised form 1 July 2013
Accepted 13 July 2013
Available online 20 July 2013

Keywords:
Nanocontainers
Ultrasonic irradiations
LbL assembly
Corrosion inhibitor
Release rate

ABSTRACT

The present work deals with the loading and responsive release of corrosion inhibitor (benzotriazole) on polyelectrolyte layer in the case of anticorrosive nano pigment calcium zinc phosphate [$CaZn_2(PO_4)_2$] prepared by layer-by-layer (LbL) method. Synthesis of $CaZn_2(PO_4)_2$ and the encapsulation of polyaniline (PANI) on nano $CaZn_2(PO_4)_2$ and LbL assembly of nanocontainers has been achieved using ultrasonic irradiation. Formation of small/uniform particle size of nanopigment and complete encapsulation of polyelectrolyte on the pigment has been observed mainly due to the presence of ultrasonic irradiations during the preparation process. The release of benzotriazole from $CaZn_2(PO_4)_2$ nanocontainer have been quantitatively evaluated in water at different pH. With an increase in the percent loading of $CaZn_2(PO_4)_2$ nanocontainer from 0 to 4%, the corrosion rate has been found to be decreased from 2.2 to 0.15 mm/y respectively in 5% HCl. Corrosion potential values are found to be shifted to positive side from −0.62 to −0.485 V with the addition of 4 wt.% of $CaZn_2(PO_4)_2$ nanocontainers in the alkyd resin. Results of corrosion rate analysis, Tafel and Bode plots of nanocontainer coatings on mild steel panel showed significant improvement in the anticorrosion performance of the nanocontainer/alkyd resin coatings.

1. Introduction

Pigments such as lead and chromates are not preferred in the surface coating formulations due to the environmental reasons and are now being replaced by the eco friendly pigments. Such pigments include phosphate based pigments among which zinc phosphate has been found to have wide range of application due to its non-toxic nature, excellent anticorrosive properties and can be readily used in the coatings [1–4]. Recently, the pigments containing the basic phosphates and its modifications with cations and anions such as Zn, Si, Ca, Fe, K have been depicted as modified eco-friendly pigments. This modification can enhance the corrosion inhibition efficiency and make water insoluble complex leading to an enhancement in the anticorrosion property. Few literature illustrations also report modified phosphate pigments using organic moieties such as long chain organic modifiers on organo-clay or nanoclay. Functionalization of phosphate compounds by addition of organic moieties is a recent technology in anticorrosion coatings; however, the important requisite is that the surface of metal should be compatible for silane coupling. Recent works also report the additions of ions such as cation like calcium, potassium, aluminum etc. during preparation of nanopigments, which are being used as anticorrosion pigments in the surface coating industry ranging in the micrometer size [5–9]. Only few reports illustrate the synthesis of calcium zinc phosphate in nanosize range [10]. Inherently, zinc phosphate pigment has low anticorrosion property due to low solubility. Anticorrosion performance of zinc phopshate pigment can be intensified by modifying the zinc phosphate pigment by an addition of cations such as calcium, potassium, aluminum or anions such as SiO_4 and MoO_4^{3-} [10,11].

* Corresponding author. Tel.: +91 870 2462626.
E-mail address: shirishsonawane@rediffmail.com (S.H. Sonawane).

1385-8947/$ - see front matter © 2013 Elsevier B.V. All rights reserved.
http://dx.doi.org/10.1016/j.cej.2013.07.030

Use of ultrasonic irradiations has been proved to be a useful tool for intensification of the synthesis of nanoparticles [12]. The chemical effects of ultrasonic irradiation arise from acoustic cavitation, which can be described as the formation, growth and implosive collapse of bubbles in a liquid medium resulting in the generation of high temperature and pressure pulse and intense turbulence associated with liquid circulation currents [13,14]. These extreme conditions of high temperature, pressure and local intense micromixing helps in the formation of nanoparticles with near-uniform size distribution [12,15]. With this background, the synthesis of calcium zinc phosphate is investigated in the presence of ultrasound, which is expected to assist the dissolution of precursor of zinc phosphate and generate final particles with smaller size with narrow size distribution. Further, if the calcium zinc phosphate particle size is reduced to nanosize range, it is expected to show a better effect on the anticorrosion properties of coatings based on calcium zinc phosphate [10].

Encapsulation of active materials loaded on the inorganic core is one of recent technique, for the storage and release of liquid corrosion inhibitor on the demand, described as "nanocontainers" which could be loaded on the organic coating formulations [16–23]. The important advantages offered by the incorporation of these containers into organic coatings are as follows, (1) responsive and sustainable release of inhibitor as a function of pH or temperature (2) if the liquid inhibitors cannot be used directly in the coatings formulation due to possible reaction of these inhibitors with the coating, encapsulation method can be used to prepare the reservoir of inhibitors in micro or nano-container. In order to achieve the dual advantage of the anticorrosive pigment (core of nanocontainer) and inhibitor loaded on the inorganic core, calcium zinc phosphate has been used as a core of the nanocontainer formulation, which works as a cathodic inhibitor controlling the cathodic reactions as well as a good nano-filler. Nanosize calcium zinc phosphate may significantly inhibit the corrosion of the bare steel by a cathodic protection mechanism, which is also enhanced due to an increase in its surface area (due to the reduction in the size to nano-range). Also the protection of metal substrate is given by cathodic inhibition properties of Zn^{2+} by precipitation at cathode (reduction of O_2 to HO^-) and thereby preventing the direct contact between the metal surface and potentially aggressive species such as O_2, H_2O, Cl^- etc. and hence metal surface is protected.

The current work reports an innovative attempt to prepare nanocontainer using calcium zinc phosphate. The main aim of this study was to intensify the synthesis of nano-pigment in the form of layer by layer assembly using ultrasound and to evaluate the anticorrosive properties of calcium zinc phosphate nanocontainer. The calcium zinc phosphate pigment was innovatively prepared through ultrasound assisted co-precipitation technique. Further studies involved the preparation of nanocontainers using the calcium zinc phosphate pigment as a core and loading these containers into the alkyd resin at different concentrations. The release of the benzotriozole inhibitor from the Layer by Layer (LbL) assembly of calcium zinc phosphate nanocontainers incorporated in alkyd resin has also been investigated. One of the prospective applications of these nanocontainers could be for the corrosion protection in the oil and gas field and marine equipment applications.

2. Experimental

2.1. Materials

Analytical grade chemicals such as zinc oxide (ZnO), calcium hydroxide ($Ca(OH)_2$), phosphoric acid (H_3PO_4), ammonium persulphate (APS, $(NH_4)_2S_2O_8$, inhibitor) and sodium dodecyl sulfate (SDS, $NaC_{12}H_{25}SO_4$, surfactant) were procured from S.D. Fine Chem. and used as received without further purification. Analytical grade chemicals such as sodium hydroxide, benzotriazole, HCl, NaOH, NaCl and ethanol, polyacrylic acid (PAA, M_w = 50,000 g mol^{-1}) were procured from Sigma Aldrich. The monomer aniline (analytical grade, M/s Fluka) was distilled two times prior to the use. Demineralized water prepared using Millipore apparatus was used during all the experimental runs.

2.2. Concept of preparation of $CaZn_2(PO_4)_2$ nanocontainer

Fig. 1 depicts the mechanism of $CaZn_2(PO_4)_2$ nanocontainer synthesis process. As shown in Fig. 1, initially the $CaZn_2(PO_4)_2$ nanoparticles are functionalized with Myristic acid (MA), which improves the hydrophobicity of the $CaZn_2(PO_4)_2$ nanoparticles and subsequently, negatively charged $C_{13}H_{27}COO^-$ ions gets adsorbed on the surface of $CaZn_2(PO_4)_2$ nanoparticles. Due to the hydrophobicity of MA coated $CaZn_2(PO_4)_2$ nanoparticles and developed negative charge on $CaZn_2(PO_4)_2$ nanoparticles, the deposition of PANI layer on $CaZn_2(PO_4)_2$ nanoparticles is successfully accomplished in the next step. Further, adsorption of second layer of benzotriazole molecules is obtained on the PANI encapsulated calcium zinc phosphate nanoparticles. Finally, adsorption of the negatively charged PAA layer is accomplished after the formation of the layer of benzotriazole. Use of ultrasonic irradiations in all the depositions of PANI, benzotriazole and PAA layer results in the distinct formation of $CaZn_2(PO_4)_2$ nanocontainer particles with an increased component diffusivity meeting the requirements of the particle size and uniform coating/layer formation.

2.3. Ultrasound assisted preparation of $CaZn_2(PO_4)_2$ and nanocontainers

Synthesis of $CaZn_2(PO4)_2$ has been carried out by using ultrasound assisted chemical precipitation method. Initially, aqueous solution of calcium zincate was prepared by chemical reaction between 2.2 g zinc oxide and 4.8 g calcium hydroxide prepared in 250 mL deionized water in the presence ultrasonic irradiation (ultrasonic horn operating at frequency of 22 kHz and power as 240 W) and magnetic stirring for 20 min. The reaction mass was then heated to 60 °C and reaction temperature was maintained throughout the experimentation. Drop-wise addition of stoichiometric amount of dilute H_3PO_4 to the above prepared mixture was accomplished within 30 min in the presence of ultrasound irradiation and further reaction was continued for additional 30 min (total reaction time being 60 min). Synthesis of $CaZn_2(PO4)_2$ nanocontainers have been carried out in a stepwise manner as described below:

2.3.1. Preparation of PANI encapsulated nano $CaZn_2(PO_4)_2$

During the synthesis of $CaZn_2(PO_4)_2$ nanocontainer by LbL method, $CaZn_2(PO_4)_2$ was used as core because of its excellent anticorrosion properties due to the presence of Zn and phosphate moieties. $CaZn_2(PO_4)_2$ nanoparticles were initially functionalized using the myristic acid by adding 0.2 g myristic acid (MA) in 10 mL methanol and then adding it subsequently in the aqueous solution containing $CaZn_2(PO_4)_2$ (1 g in 100 mL water) at 60 °C. The mixture was then irradiated using ultrasonic horn for 60 min. Myristic acid functionalization generates negative charges on the surface of $CaZn_2(PO4)_2$. Encapsulation of MA functionalized $CaZn_2(PO_4)_2$ (core) by positively charged PANI layer has been accomplished by ultrasound assisted in situ emulsion polymerization [24]. Initially, surfactant solution was prepared by adding 3 g of SDS and 0.2 g of MA modified $CaZn_2(PO_4)_2$ in 50 mL water, which was subsequently transferred to an ultra-

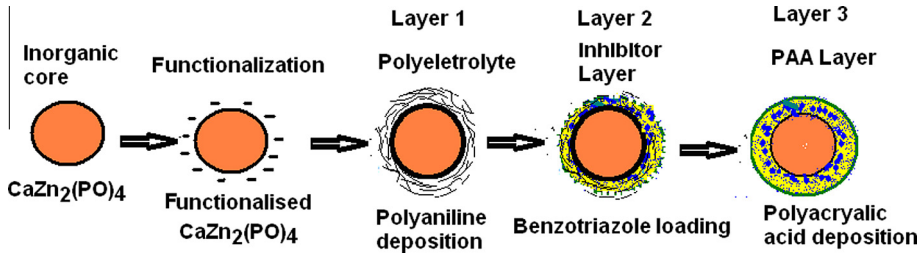

Fig. 1. Schematic illustration of the procedure for synthesis of $CaZn_2(PO_4)_2$ nanocontainer.

sound reactor. Initiator solution was prepared independently by adding 3.5 g ammonium persulphate (APS) in 20 ml of deionized water and then added to the reactor. Further, drop wise addition of a total quantum of aniline as 5 g was achieved over a period of 30 min. After complete addition of aniline, the entire reaction mixture was sonicated in reactor at 4 °C temperature throughout the reaction time of 1.5 h. Formed PANI coated $CaZn_2(PO_4)_2$ nanocontainer particles were separated by centrifugation and then washed with water. The separated product was dried at 60 °C in oven for 4 h.

2.3.2. Benzotriazole layer loading on PANI-$CaZn_2(PO_4)_2$

PANI encapsulated $CaZn_2(PO_4)_2$ materials (2 g) was added into 0.1 N NaCl solution prepared in 100 mL water. Further, loading of positively charged benzotriazole layer on the surface of PANI encapsulated $CaZn_2(PO_4)_2$ nanoparticles was accomplished using 2 mg mL^{-1} of benzotriazole in acidic media at pH 3 in ultrasound assisted environment for 20 min. Benzotriazole loaded PANI-$CaZn_2(PO_4)_2$ nanoparticles were separated by centrifugation and used for further PAA layer loading.

2.3.3. PAA loading on benzotriazole-PANI-$CaZn_2(PO_4)_2$ Particles

In order to get a response due to the change in the pH and to make nanocontainers compatible to resin, polyacrylic acid polyelectrolyte layer was added after the loading of benzotriazole on PANI layer. PAA polyeletrolyte deposition was carried on benzotriazole loaded PANI-$CaZn_2(PO_4)_2$ nanoparticles using 2 mg mL^{-1} PAA solution in 0.1 N NaCl in the presence of ultrasound irradiation for 20 min. Finally, the resulting $CaZn_2(PO_4)_2$ nanocontainer particles were centrifuged and then dried in oven at 60 °C for 48 h. Thus, LbL assembly consists of MA modified $CaZn_2(PO_4)_2$ as core of the assembly and benzotriazole inhibitor was loaded in between the layers of PANI and PAA.

2.4. Preparation of $CaZn_2(PO_4)_2$ nanocontainer/alkyd coatings

Preparation of $CaZn_2(PO_4)_2$ nanocontainers/alkyd coatings has been accomplished by dispersing 2.0 and 4.0 wt.% of freshly prepared $CaZn_2(PO_4)_2$ nanocontainers in Soya alkyd resin (total quantity as 10 g). Dispersion of these nanocontainers is achieved using automatic pigment muller. The prepared coating was thoroughly mixed with acetone solution to ease the application of coating by using bar coater on mild steel panels having dimensions 50 × 40 × 1 mm.

2.5. Characterization of prepared nanocontainer and coatings

XRD diffraction patterns of $CaZn_2(PO_4)_2$ and $CaZn_2(PO_4)_2$ nanocontainer were recorded by using powder X-ray diffractometer (Philips PW 1800). The morphology of $CaZn_2(PO_4)_2$ nanocontainer was established using transmission electron microscopy (TEM) (Technai G20 working at 200 kV) and atomic force microscopy (AFM). Release of corrosion inhibitor benzotriazole at different pH was measured using UV–vis spectrophotometer (SHIMADZU 160A model). Initially the calibration curve was plotted for different concentrations over the range 0.01–1 mg/L of Benzotriozole. Proportionate benzotriazole release in water was calculated from the absorbance. The concentration of benzotriazole was reported in mg of benzotriazole released per g of nanocontainer added per liter of water. FTIR analysis of samples was carried out (SHIMADZU 8400S) in the region of 4000–500 cm^{-1}. The particle size distribution and Zeta potential measurements were carried out by Malvern Zetasizer Instrument (Malvern Instruments, Malvern, UK).

Corrosion tests were conducted in acid, alkali, and salt solution (5 wt.% each) by the dip test method without putting any scratch on the panel. The thickness of the coating film on MS plate was around 50 μm. Corrosion tests were conducted for different samples under salt and acidic medium for nearly 250 h and 175 h respectively. The protective behavior of corrosion inhibitor against the dissolution of MS was evaluated by calculating the corrosion rate (V_c) in mm/year for each samples [24] by using the following expression.

$$V_c = \frac{\Delta g}{Atd} \quad (1)$$

where Δg is the weight loss in gram for each sample, A is the exposed area of the sample in mm^2, t is the time of exposure in years, and d is the density of the metallic species in g/mm^3. The weight loss was measured after carefully washing the samples with water till the deposited corrosion products were removed, and finally, moisture was removed from the samples by drying the same at 60 °C (±1) in an oven till constant weight is obtained.

Electrochemical corrosion analysis (Tafel plot ($\log|I|$ vs. E)) was carried out in 5% NaCl solution as an electrolyte at room temperature (25 °C). All measurements were performed on computerized electrochemical analyzer (Autolab Instruments, Netherlands). Three different MS plates coated with neat alkyd resin, 2 and 4 wt.% $CaZn_2(PO_4)_2$ nanocontainer dispersed in the same alkyd resin were used as working electrode, while Pt and Ag/AgCl were used as counter and reference electrodes respectively. The area of about 1 cm^2 was used for sample testing. The electrochemical window was −1.0 V to +1 V with 2 mV/s scanning rate. Electrochemical impedance spectroscopy (EIS) of neat alkyd resin, alkyd resin–$Ca(Zn)_2(PO_4)_2$ nanoparticles (prepared by ultrasound and conventional method) and alkyd resin-nanocontainer coated mild steel panel (130 mm × 100 mm × 1 mm) was carried out to assess the corrosion phenomena and corrosion inhibition mechanism of the coating based on nanocontainer in a 3.5 wt.% NaCl solution (at 25 °C). A three-electrode set-up was used to measure corrosion potential of coating. A saturated calomel electrode was used as the reference electrode. It was coupled capacitively to a Pt wire to reduce the phase shift at higher frequencies. Electrochemical impedance tests were carried out by using Versa STAT 3 provided with frequency response analyzer, with varying frequency in the range from 1 Hz to 100 kHz to collect data recorded in terms of Bode plot.

3. Results and discussions

3.1. Particle size and zeta potential analysis of $CaZn_2(PO_4)_2$ nanocontainers

Zeta potential analysis (Electrophoretic measurements) indicates the change in charge on the nanoparticles surface due to the addition of each layer. The layer-by-layer (LbL) nanocontainer assembly preparation procedure was monitored by measuring the electrophoretic mobility (ζ-potential) in water after each layer was added.. Fig. 2a shows the zeta (ζ) potential value after each layer deposition in the LbL assembly of nanocontainer. The surface charge of $CaZn_2(PO_4)_2$ nanoparticles is about 32.8 mV. Fig. 2a, shows a drastic decrease in the surface charge after deposition of the first PANI layer (about – 61.9 mV). This drastic change may be due to the presence of SDS which is adsorbed on the $CaZn_2(PO_4)_2$ during in situ emulsion polymerization. This negative value of zeta potential is higher even though PANI introduces positive charge on the surface of the nanocontainer. Further, deposition of positively charged benzotriazole (third layer) layer on the surface of PANI encapsulated $CaZn_2(PO_4)_2$ is confirmed by an increase in zeta potential value to −52.4 mV. This clearly indicates the adsorption of positively charged benzotriazole on the surface of PANI encapsulated $CaZn_2(PO4)_2$. Adsorption of positively charged polyacrylic acid (PAA) layer on benzotriazole loaded PANI-$CaZn_2(PO_4)_2$ shows further increment in the zeta potential value to −38.3 mV.

Fig. 2b depicts the increase in the size of nanocontainer in terms of particle size with the loading of each layer in LbL assembly determined by using particle size analyzer. The average particle size of $CaZn_2(PO_4)_2$ nanoparticles is found to be 53.7 nm (core size). After adsorption of PANI layer on $CaZn_2(PO_4)_2$ nanoparticles, the average particle size is observed to increase to 134.5 nm. This clearly indicates the adsorption of PANI on the surface of $CaZn_2(PO_4)_2$ nanoparticles. The thickness of the PANI layer is estimated to be 40.4 nm. Adsorption of benzotriazole layer on PANI-$CaZn_2(PO_4)_2$ leads to an increase in the average particle size further to 281.2 nm. The calculated thickness of the benzotriazole is around 73.35 nm. This is an indication of maximum adsorption of benzotriazole molecules on PANI coated $CaZn_2(PO_4)_2$ particle assembly. The chains of PAA embedded on benzotriazole layer gives rise to the formation of final $CaZn_2(PO_4)_2$ nanocontainer with particle size of 493 nm with an average thickness of PAA layer as 105.9 nm. Layer by layer deposition of PANI, benzotriazole and PAA lead to an increase in the average particle size and is attributed to the complete formation of the $CaZn_2(PO_4)_2$ nanocontainer assembly as schematically reported in Fig. 1. The average particle size of the complete layer by layer assembled $CaZn_2(PO_4)_2$ nanocontainer was found to be around 493 nm.

Further the particle size distribution of sonochemically and conventionally synthesized calcium zinc phosphate nanoparticles is reported in Fig. 3A. The range of the particle size of calcium zinc phosphate nanoparticles found is 37–78 nm in case of sonochemical synthesis, whereas it is 220–396 nm in case of conventional method and also the distribution in the presence of ultrasound showed only one narrow peak. The average particle size of calcium zinc phosphate particles observed is 53.7 nm in case of sonochemical method whereas it is 302 nm for conventional method. The particles were formed with a fairly narrow size distribution and uniform shape could be observed in the case of sonochemical synthesis. The significant reduction in the particle size of calcium zinc phosphate nanoparticles is credited to the significantly improved micromixing, enhanced solute transfer rate, rapid nucleation, and formation of large number of nuclei due to physical effects of the ultrasonic irradiation. The possible explanation for this reduction in the particle size is also the fast kinetics of the ultrasound assisted reaction, which does not give enough time for growth of particle leading to reduction in the particle size. Also the particle size distribution of nanocontainer after each layer deposition is depicted in Fig. 3B. After loading of PANI layer on $CaZn_2(PO_4)_2$ nanoparticles, the particle size is found to be in the range of 105–220 nm with maximum particles in the range of 142–190 nm indicating consistency in the size distribution of PANI loaded $CaZn_2(PO_4)_2$ particles. The loading of benzotriazole layer on PANI loaded $CaZn_2(PO_4)_2$ particles shows particle size range in between 220 and 396 nm (maximum particles are in the range of 300–396 nm). This narrow size distribution clearly indicates uniform adsorption of benzotriazole on PANI loaded $CaZn_2(PO_4)_2$ particles. Finally adsorption of PAA layer on benzotriazole loaded PANI-$CaZn_2(PO_4)_2$ particles shows particle size distribution in the range of 396 to 615 nm. The narrow particles size distribution is attributed to improved micromixing due intense implosion of cavities generated by ultrasonic irradiation.

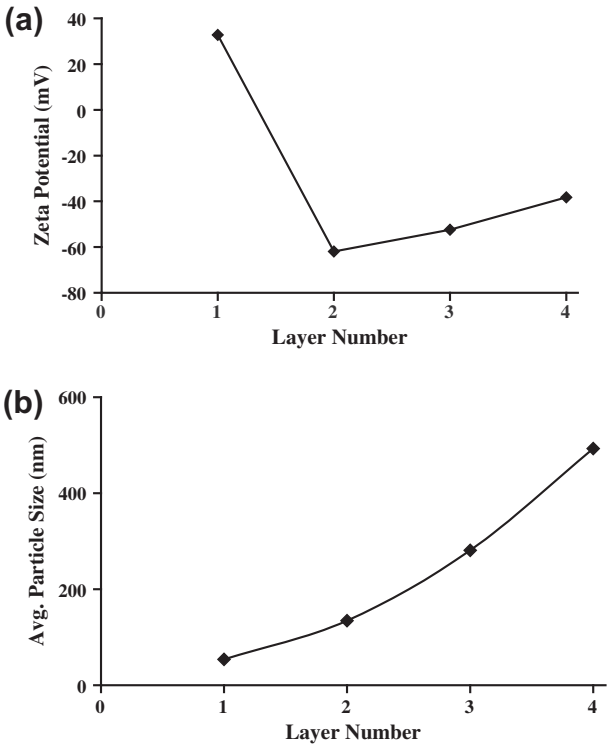

Fig. 2. (a) Electrophoretic mobility measurements and (b) growth in particle size of nanocontainer in water during LbL assembly. Layer number 1: initial $CaZn_2(PO4)_2$, 2: $CaZn_2(PO4)_2$/PANI, 3: $CaZn_2(PO4)_2$/PANI/benzotriozole, 4: $CaZn_2(PO4)_2$/PANI/benzotriozole/PAA.

3.2. Morphological analysis of $CaZn_2(PO_4)_2$ nanocontainers

Fig. 4 reports the TEM images of $CaZn_2(PO_4)_2$ nanoparticles and $CaZn_2(PO_4)_2$ nanocontainers synthesized by ultrasound assisted method. Particle size of one dimension of particle has been observed to be around 45–53 nm (Fig. 4A). The obtained results are consistent with particle size observed using the particle size distribution analysis as discussed in the earlier sections. The particle size distribution shows narrow distribution without significant agglomeration, which can be easily explained on the basis of the effects of ultrasonic irradiation. Further, the particle size is controlled by smaller induction period and better control of the growth rate of crystal because of the presence of cavitation during chemical precipitation method [12].

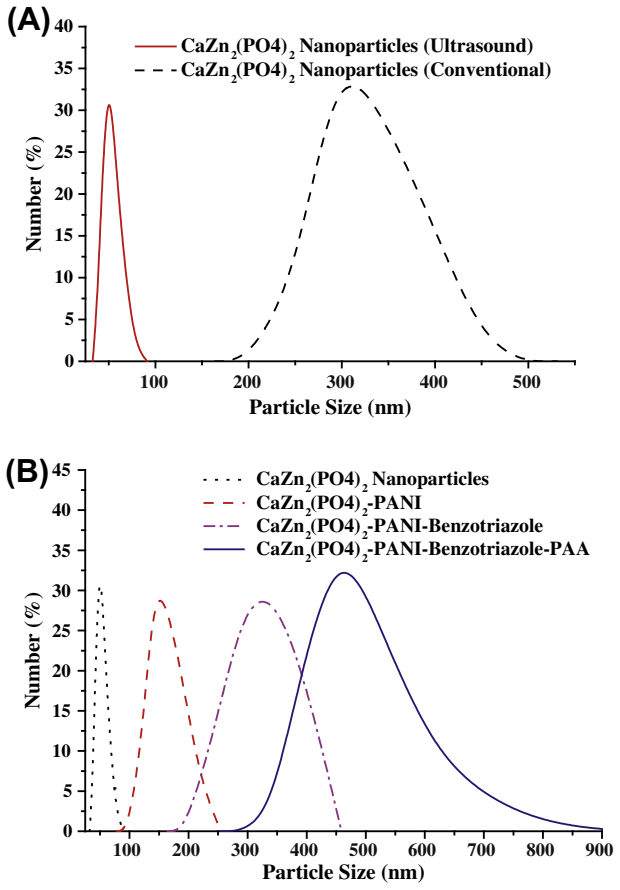

Fig. 3. Particle size distribution of (A) $CaZn_2(PO4)_2$ nanoparticles prepared by ultrasound assisted and conventional method and (B) $CaZn_2(PO4)_2$ nanoparticles, $CaZn_2(PO4)_2$/PANI, $CaZn_2(PO4)_2$/PANI/benzotriozole and $CaZn_2(PO4)_2$/PANI/benzotriozole/PAA particles prepared by ultrasound assisted method.

A transmission electron microscopy image of $CaZn_2(PO_4)_2$ nanocontainer containing $CaZn_2(PO_4)_2$ nanoparticles at core along with polyelectrolyte material surrounding the $CaZn_2(PO_4)_2$ nanoparticles is shown in Fig. 4B and Fig. 4C. The TEM images also indicate the distinct formation of $CaZn_2(PO_4)_2$ nanocontainer spheres. Further, the presence of bright intensity layered structure around the dark $CaZn_2(PO_4)_2$ nanoparticles in TEM image has confirmed the layer formation of PANI, benzotriazole and PAA. The presence of benzotriazole and polyelectrolytes around $CaZn_2(PO_4)_2$ nanoparticles results in an increase in the average particle size of $CaZn_2(PO_4)_2$ nanocontainer, to around 500 nm. These results are consistent with the average particle size of $CaZn_2(PO_4)_2$ nanocontainer obtained from the particle size analyzer (as reported in Section 3.2). Change in the scattering of light around each particles show that multilayer assembly (PANI/benzotriozole/PAA layers) is established on the $CaZn_2(PO_4)_2$ nanoparticles.

Fig. 5 shows the AFM images of $CaZn_2(PO_4)_2$ nanocontainer prepared by layer by layer deposition of PANI, Benzotriazole and PAA. Fig. 5a reveals the topography of the nanocontainer showing the presence of spherical particle like features with a diameter of about 500 nm [25]. The surface relief profiles are also reported in Fig. 5b which has been obtained through AFM analysis. This profile shows layered structure of $CaZn_2(PO_4)_2$ nanocontainer. It has been confirmed from AFM image that formed $CaZn_2(PO_4)_2$ nanocontainer shows two layer structure; one organic layer (due to PANI, Benzotriazole and PAA) and second an inorganic core because of $CaZn_2(PO_4)_2$ nanoparticles [25].

3.3. FTIR analysis of $CaZn_2(PO_4)_2$ nanocontainers

Fig. 6 depicts the FTIR spectrum of calcium zinc phosphate nanocontainer at different steps during synthesis of the nanocontainer. Fig. 6A presents the FTIR spectrum of calcium zinc phosphate used as a core during synthesis of nanocontainer. The prominent peak at 570–611 and 1051 cm^{-1} is assigned to the vibration modes of PO_4^{3-} (amorphous calcium zinc phosphate) [26–28]. A small peak at 1222 cm^{-1} originated from symmetric stretching of PO_4^{3-} red-shifted from the reference peak. In the next step in the synthesis approach, ultrasound assisted synthesized calcium zinc phosphate is modified with myristic acid (MA) and the FTIR spectrum of the MA modified calcium zinc phosphate is depicted in Fig. 6B. In addition to the peaks of calcium zinc phosphates, the characteristic peaks at 2920 and 2848 cm^{-1} shows stretching vibration of the C—H which came from the —CH_3 and —CH_2 groups in the myristic acid respectively. Further characteristic peak at 1541 cm^{-1} is attributed to bending of —OH. In the Fig. 6C, characteristic peak at 1149 cm^{-1} are due to the (C—N) stretching mode of the amine group of PANI. The characteristic peak at 1498 cm^{-1} represents C=C stretching mode of the quinoid rings and C=C stretching of benzenoid rings respectively [29]. The characteristic peak at 1560 cm^{-1} corresponds to the secondary =N—H bending. The presence of characteristic peaks of polyaniline confirms the formation of polyaniline on the surface of calcium zinc phosphate nanoparticles. The FTIR spectrum after loading of benzotriazole on PANI loaded MA modified calcium zinc phosphate is reported in Fig. 6D. The characteristic peaks at 1251, 1188, 1157 and 759 cm^{-1} indicates the formation of the benzotriazole layer of PANI coated calcium zinc phosphate. The bands close to 759 cm^{-1} are typical of the benzene ring vibration and the band near to 1467 cm^{-1} is characteristic of the aromatic and the triazole ring stretching vibrations [30]. Finally, Fig. 6E shows the FTIR spectrum of the calcium zinc phosphate nanocontainer after PAA layer adsorption. The characteristic bands at 1718 cm^{-1} are for the PAA carbonyl C=O stretching [31].

3.4. XRD analysis of $CaZn_2(PO_4)_2$ nanocontainers

Fig. 7 shows the X ray diffraction patterns of the calcium zinc phosphate nanoparticles and its nanocontainer. As shown in Fig. 7A, the formation of crystalline $CaZn_2(PO_4)_2$ was confirmed by X Ray diffraction analysis. The X-ray diffraction pattern of the product has been matched with $CaZn_2(PO_4)_2$–$2H_2O$ in JCPDS file (Card No. 35-0495). Diffraction peaks at 25.9°, 29.4°, 31.8°, 34.4°, 36.4°, 47.6°, 56.6°, 62.9° and 68° correspond to pure calcium zinc phosphate without the presence of the reactants and calcium zincate media ($Ca[Zn(OH)_3]_2{\cdot}2H_2O$). As no peaks of impurity have appeared in X-ray diffraction, the formation of pure calcium zinc phosphate nanoparticles can be confirmed. The crystallite size is calculated based on the major peak which is observed at 36.4° (2 Theta angle). The calculated crystallite size of calcium zinc phosphate nanoparticles using Scherrer's formula is about 10 nm. Similar results have been reported by the Ding and Wang [10]. Fig. 7B shows the XRD of calcium zinc phosphate nanocontainer, in which no characteristic peak of calcium zinc phosphate is being observed indicating that the calcium zinc phosphate nanoparticles are completely covered by corrosion inhibitor and polyelectrolyte layers. The change in the intensity value also indicates the complete coverage of calcium zinc phosphate nanoparticles by the long chain organic molecules. It is also predicted that due to deposition of polyelectrolyte and benzotriazole layers on calcium zinc phosphate, the structure and phase of calcium zinc phosphate has not

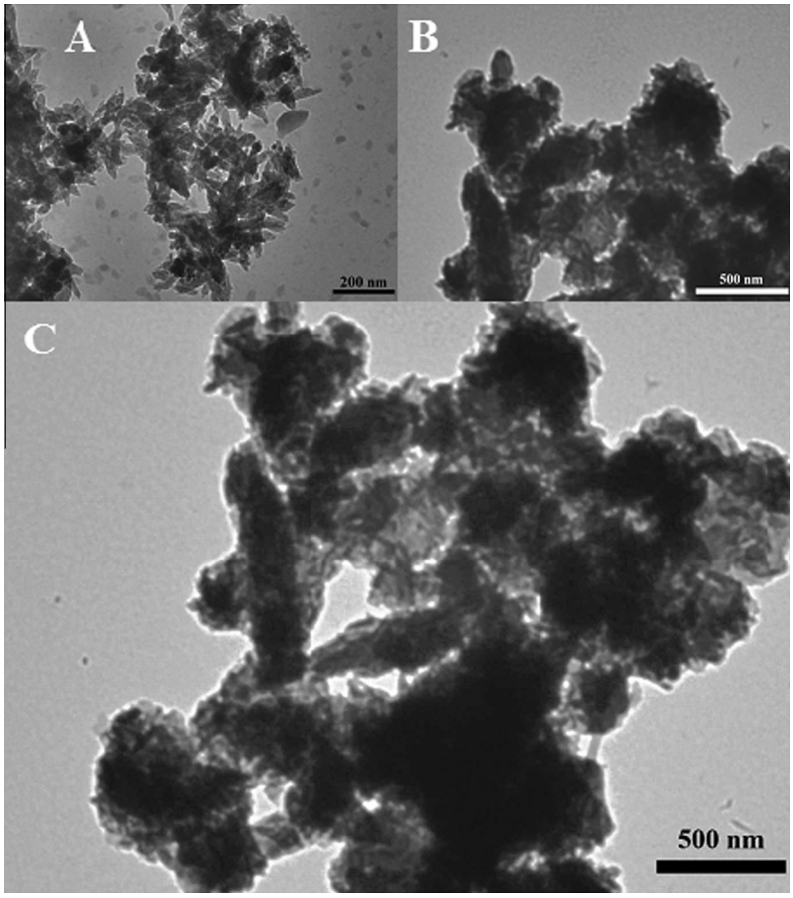

Fig. 4. TEM Image of (A) $CaZn_2(PO_4)_2$ nanoparticles, (B and C) $CaZn_2(PO_4)_2$ nanocontainer.

been detected. Further flattening and broadening of X-ray diffraction patterns of calcium zinc phosphate nanoparticles with the loading of organic layers are due the change in the crystallinity of calcium zinc phosphate nanoparticles present at the core indicating that calcium zinc phosphate nanoparticles are no longer in crystalline phase.

3.5. Release study of corrosion inhibitor

In order to investigate the responsive release of benzotriozole from nanocontainer assembly and sensitivity of nanocontainers to different ionic strength, a series of release experiments were carried out in aqueous solutions of different pH. The pH was adjusted by adding either dilute acid (HCl) or alkali solution (NaOH). Objective of the investigation was to validate the mechanism of responsive release and also to find the optimum pH conditions at which the release reaches a maximum value. Fig. 8 depicts the release concentration of corrosion inhibitor, benzotriazole, per unit mass of calcium zinc phosphate nanocontainer at different pH. It has been observed that, initially the extent of release increases rapidly and after a certain time the concentration is mostly constant. It has been reported that the benzotriazole acts as an inhibitor for ferrous metals under acidic conditions [32–34] and neutral conditions [35,36]. In acidic conditions, the inhibition of ferrous metal is due to the adsorption of benzotriazole in its molecular or protonated form along with the formation of compact passive layer [34]. Further, it has been found that benzotriazole gives better corrosion inhibition in acidic medium. With this objective the release performance of the benzotriazole containing nanocontainers have been studied in aqueous media of pH 3, 5, 7 and 9, which was adjusted using buffer solutions. It is found that the release is reduced with an increase in the pH value. The amount of released corrosion inhibitor (benzotriazole) is more in acidic pH compared to neutral and alkaline pH. The higher release in the acidic medium results into quick formation of compact passive layer by the chemisorption of benzotriazole in its molecular or protonated form leading to an improvement in the inhibition of ferrous metal compared to neutral as well as alkali medium. The maximum release concentration of benzotriazole at the end of 4 h is 0.393 mg L^{-1}/g of $CaZn_2(PO_4)_2$ nanocontainer, which is found in the case of solution having a pH of 3. Further the release concentration is found to be 0.372, 0.354 and 0.34 mg L^{-1}/g of $CaZn_2(PO_4)_2$ nanocontainer at 5, 7 and 9 pH value respectively. More the release of corrosion inhibitor better will be the protection of ferrous metal with quick formation of compact passive layer by the chemisorption of benzotriazole. More release of benzotriazole takes place in acidic medium and it decreases with an increase in the pH value, indicating that the corrosion protection for ferrous metal is more in the acidic medium and decreases with an increase in the pH value.

3.6. Corrosion rate analysis of $CaZn_2(PO_4)_2$ nanocontainer/alkyd coatings

Corrosion of ferrous metals is known to be pH dependent. The attack of acid or alkali leads to the hydrolytic degradation of polymer material or chain scission and chemical reactions and this may facilitate the attack of oxygen and moisture through the film. The chemical change leads to a reduction in the compactness of the film, which results into an increase in the corrosion rate. Further, the strong corrosion resistance requires strong adhesion character-

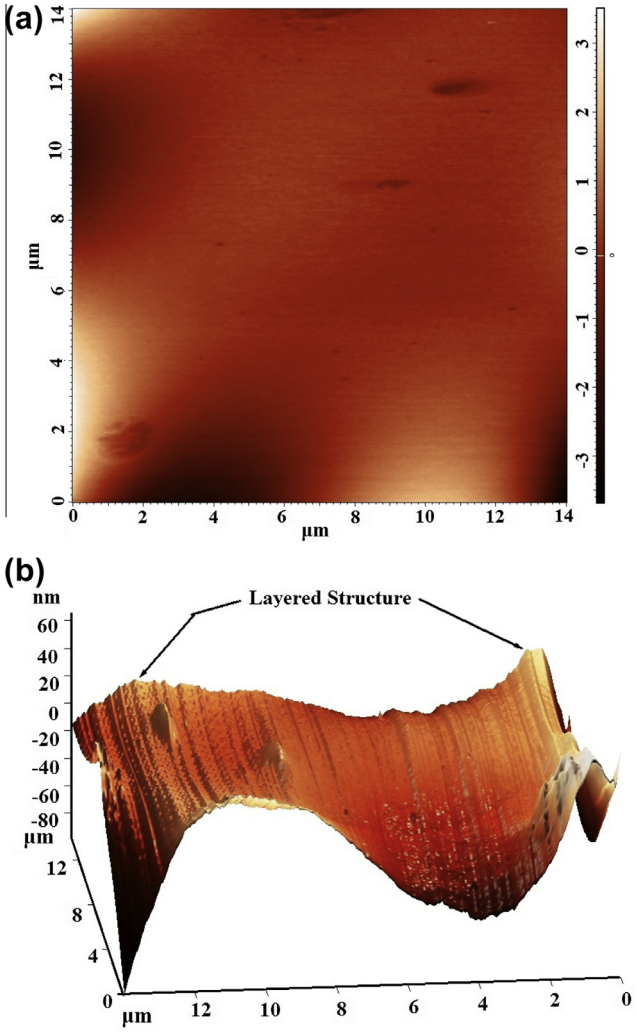

Fig. 5. Determination of the shell thickness of $CaZn_2(PO_4)_2$ nanocontainer with AFM: (a) top view; (b) surface relief profile of (a).

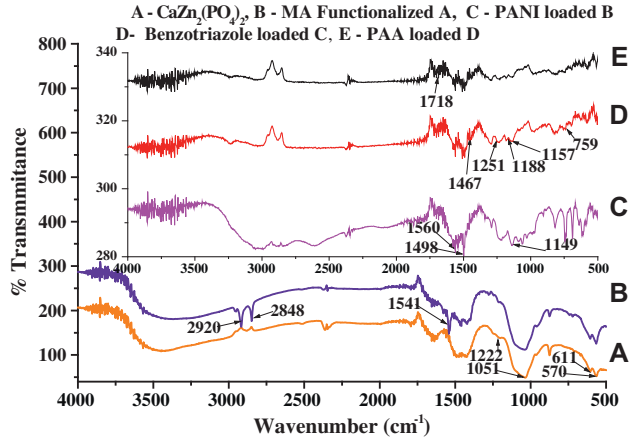

Fig. 6. FTIR spectra of: (A) $CaZn_2(PO_4)_2$, (B) MA functionalized $CaZn_2(PO_4)_2$, (C) $CaZn_2(PO_4)_2$ loaded with PANI, (D) $CaZn_2(PO_4)_2$ loaded with PANI and benzotriazole and (E) $CaZn_2(PO_4)_2$ loaded with PANI, benzotriazole and PAA (polyacrylic acid).

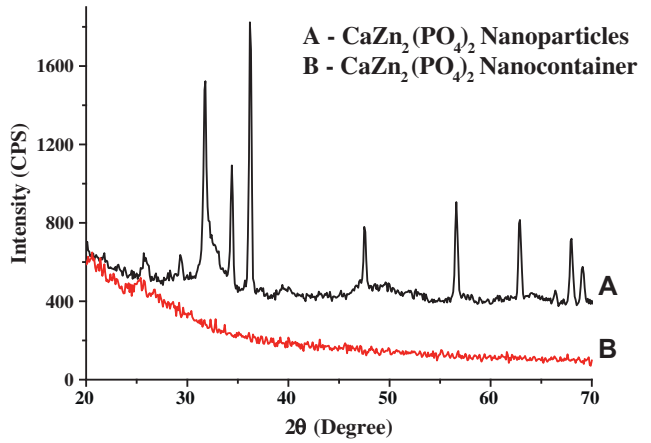

Fig. 7. XRD pattern of: (A) $CaZn_2(PO_4)_2$ and (B) $CaZn_2(PO_4)_2$ loaded with polyelectrolytes and inhibitor.

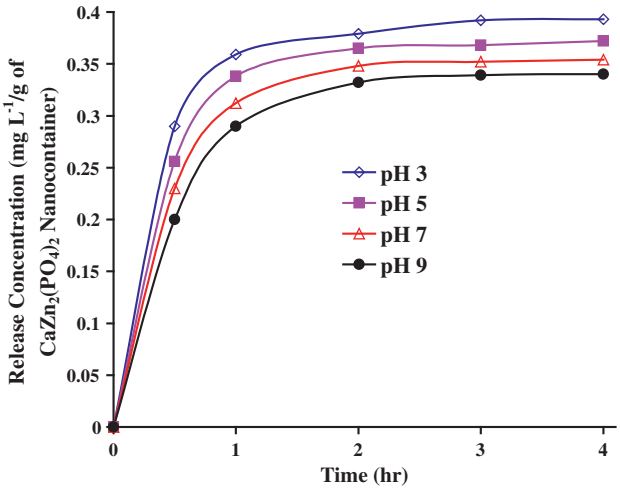

Fig. 8. Release of benzotriazole from $CaZn_2(PO_4)_2$ nanocontainers at different pH values.

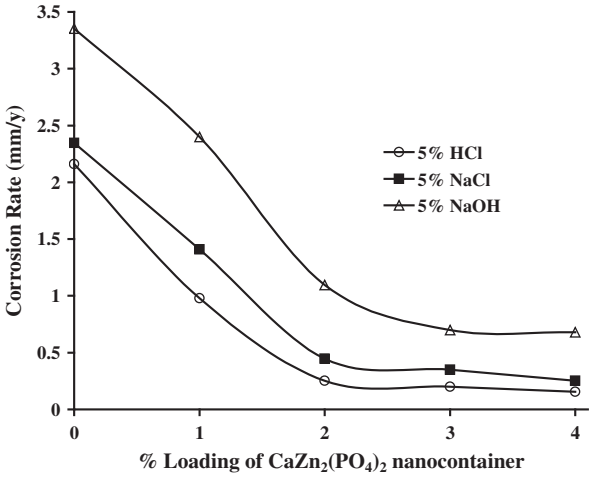

Fig. 9. Effect of loading of $CaZn_2(PO_4)_2$ nanocontainer on the corrosion rate after loading into the Alkyd resin.

istics and hence the weight loss method can be used for the evaluation of corrosion resistance. The layer by layer synthesized $CaZn_2(PO_4)_2$ nanocontainer were incorporated in alkyd resin and were coated on mild steel (MS) panels for dip test analysis. MS panels were dipped in 5% HCl, NaCl and NaOH solutions for a period of 250 h. The corrosion rate was determined by gravimetric

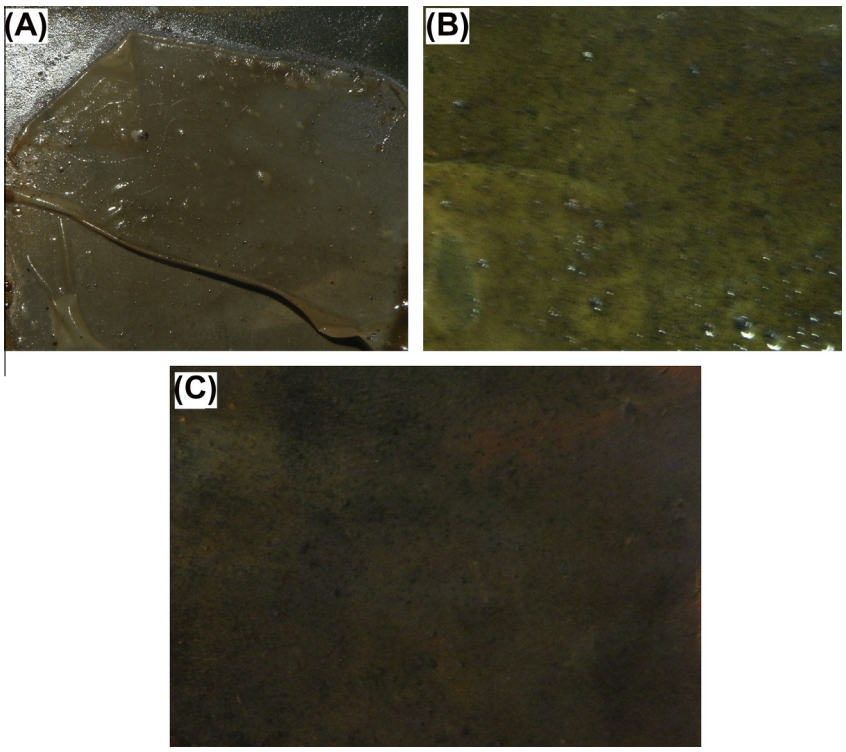

Fig. 10. Physical observations of $CaZn_2(PO_4)_2$ nanocontainer/alkyd resin coatings applied on MS panel at: (A) 0 %, (B) 2 %, and (C) 4 % loading of $CaZn_2(PO_4)_2$ nanocontainer in alkyd resin in acidic environment (HCl solution).

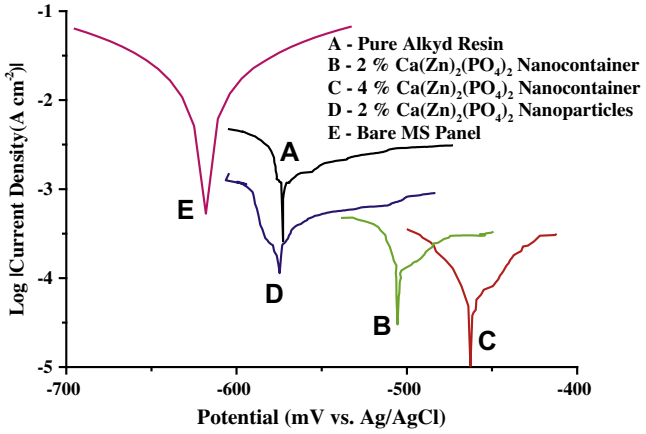

Fig. 11. Tafel plots of mild steel samples coated with different composite material in 5 wt.% NaCl solution.

analysis [24]. The corrosion rate as a function of percent loading of $CaZn_2(PO_4)_2$ nanocontainer has been given in the Fig. 9. The corrosion rate at 0% loading of $CaZn_2(PO_4)_2$ nanocontainer is found to be 2.2, 2.4 and 3.4 mm/y in case of 5% HCl, NaCl and NaOH solution respectively. Further, it has been observed that the corrosion rate (mm/y) is more in the case of alkali environment, which is attributed to insufficient passivation resulting from the lower release of benzotriazole (corrosion inhibitor) in alkali environment. Also, the anticorrosion performance increased with an increase in the loading of $CaZn_2(PO_4)_2$ nanocontainer. From Fig. 9, it has been observed that the corrosion rate is reduced with an increase in the $CaZn_2(PO_4)_2$ nanocontainer loading in all the cases i.e. 5% HCl, NaCl and NaOH solution. With an increase in the percent loading of $CaZn_2(PO_4)_2$ nanocontainer from 0% to 4%, the corrosion rate is found to reduce from 2.2 to 0.15, 2.4 to 0.25 and 3.4 to 0.67 mm/y respectively in 5% HCl, NaCl and NaOH solutions. This may be due to the sufficient passivation resulting from the enhanced release of benzotriazole (corrosion inhibitor), sacrificial nature of zinc and compactness of the coating film due to the presence of enhanced calcium. The corrosion rate is found to be significantly less in the case of acid environment (HCl solution) compared to alkali (NaOH solution) indicating that the ferrous metal is not exposed to HCl attack due to better passivation of the substrate (release of enhanced quantum of corrosion inhibitor, benzotriazole). This improved passivation results into a reduction in the corrosion rate in the acidic environment. It is also important to note that the alkyd resin and PAA (outer layer of the nanocontainer) selected during the synthesis of nanocontainer and subsequently in the coatings are acidic in nature, which helps in increase in the corrosion inhibition. It is well known that the reaction rate between acid and alkali is significant, which leads to a maximum corrosion rate of the coating in the presence of NaOH solution.

The visual observation of the MS panels such as growth of cracks that leads to a fracture, color[1] change and removal of coating at different loading of $CaZn_2(PO_4)_2$ nanocontainer in alkyd resin in acidic environment has been shown in Fig. 10. At 0 % loading of $CaZn_2(PO_4)_2$ nanocontainer, complete removal of the coating film has been observed. This indicates that the corrosion rate and infiltration of corrosion ion are significant in absence of nanocontainer, which results into the removal of the epoxy coatings. At 2% loading of the $CaZn_2(PO_4)_2$ nanocontainer in alkyd resin, an improvement in the corrosion resistance has been observed, however some blisters are still observed. Finally, at 4% loading of $CaZn_2(PO_4)_2$ nanocontainer in the alkyd resin, no change in the visual observation of the applied coating is observed even in the 5% HCl solution. This clearly confirms the improvement in the corrosion resistance with an in-

[1] For interpretation of color in Fig. 10, the reader is referred to the web version of this article.

crease in the percent loading of $CaZn_2(PO_4)_2$ nanocontainer in alkyd resin.

3.7. Electrochemical characterization of $CaZn_2(PO_4)_2$ nanocontainer/alkyd coatings

Fig. 11 shows the Tafel plot generated for different samples immersed in 5 wt.% aqueous NaCl solutions (Bare MS panel, neat alkyd resin sample, the samples coated with 2 and 4 wt.% of $CaZn_2(PO_4)_2$ nanocontainer and the sample coated with 2 wt.% of $CaZn_2(PO_4)_2$ nanoparticles dispersed in alkyd resin coated on MS panel). In corrosion process for any redox system, cathodic and anodic reactions occur simultaneously. The Tafel plot (E as a function of $\log(|I|)$, where I represents the total measured current density = $I_c + I_a$) can isolate these two processes. Using the standard analysis method, the linear portions of curves are fitted, yielding the theoretical anodic and cathodic currents. The coordinates of the intersection of these fits are the corrosion current density, I_{corr} and corrosion potential, E_{corr}. These I_{corr} and E_{corr} values were calculated from the intersection of coordinates of the Tafel plot. It is found that the electrochemical current density for bare MS panel is 0.18 A/cm^2 and E_{corr} value is −0.618 V. It is found that electrochemical current density was decreased from 0.061 (for neat alkyd resin) to 0.023 A/cm^2, when 2 wt% $CaZn_2(PO_4)_2$ nanocontainers are incorporated in neat alkyd resin coatings. The current density further decreased to 0.012 A/cm^2 when loading of $CaZn_2(PO_4)_2$ nanocontainers is increased to 4 wt.%. E_{corr} values are found to be shifted to positive side from −0.57 to −0.46 V with the addition of 4 wt.% of $CaZn_2(PO_4)_2$ nanocontainers in alkyd resin. In addition to this Tafel plot of 2% $CaZn_2(PO_4)_2$ nanoparticles loading in alkyd resin is also tested. However the performance of $CaZn_2(PO_4)_2$ nanoparticles alone in the alkyd resin is poorer (I_{corr} = 0.03 A/cm^2 and E_{corr} = --0.575 V). Overall, the results of release rate, corrosion rate, and Tafel plot (polarization curve) indicates that the addition by 4 wt.% $CaZn_2(PO_4)_2$ nanocontainer in alkyd resin shows a significant enhancement in the anticorrosive properties as compared to the neat alkyd resin. Further EIS Bode plots (Log Impedance vs. Log Frequency) of mild steel coated samples with neat alkyd resin, coatings prepared by the dispersion of $Ca(Zn)_2(PO4)_2$ nanoparticles prepared by ultrasound assisted and conventional method and $Ca(Zn)_2(PO4)_2$ nanocontainers in alkyd resin are depicted in Fig. 12. Increased impendence value with an incorporation of $Ca(Zn)_2(PO4)_2$ nanocontainers in alkyd resin coatings compared to clear alkyd resin coating clearly indicates the improvement in the anticorrosion performance of the coatings. This is due to the

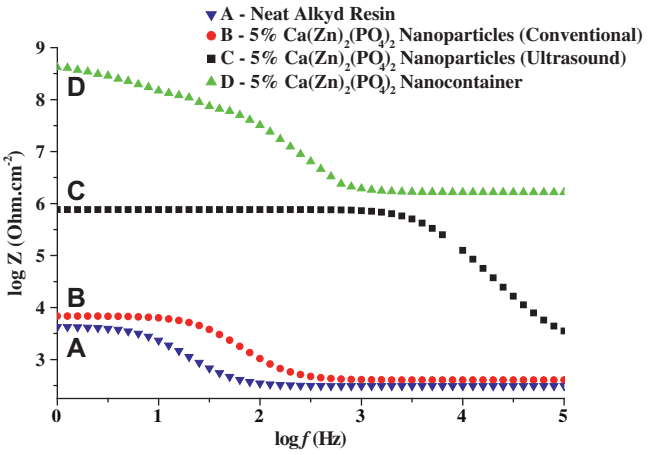

Fig. 12. Bode plots for the mild steel sample coated with (A) neat alkyd resin, (B) alkyd resin – $Ca(Zn)_2(PO4)_2$ (ultrasound) coating, (C) alkyd resin – $Ca(Zn)_2(PO4)_2$ (conventional) coating, (D) alkyd resin – $Ca(Zn)_2(PO4)_2$ nanocontainer coating, at the initial stage of immersion in 3.5% NaCl solution.

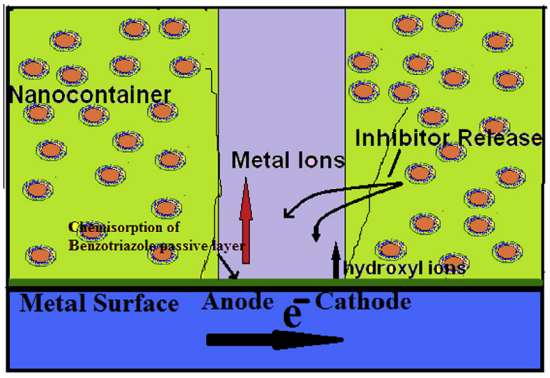

Fig. 13. Scheme of the controllable release of the inhibitor from the nanocontainers.

presence of corrosion inhibitor, which gives better resistance to corrosion process by forming and adsorbing the corrosion inhibitor i.e. benzotriazole complex on metal surface. Also particle size of $Ca(Zn)_2(PO4)_2$ has significant effect on anticorrosion performance. A comparison of anticorrosion performance of $Ca(Zn)_2(PO4)_2$ nanoparticles prepared with ultrasound assisted method dispersed in alkyd resin shows enhancement in the corrosion inhibition properties. This is attributed to decreased particle size due to ultrasonic irradiations which shows improvement in the corrosion inhibition performance compared to $Ca(Zn)_2(PO4)_2$ nanoparticles (prepared by conventional method.

3.8. Release mechanism of the inhibitor in the polymer

It has been reported that benzotriazole acts as an inhibitor for ferrous substrate under acidic [32–34] and neutral conditions [36,37]. Benzotriazole protects the surface of ferrous metal from corrosion by chemisorption of benzotriazole at the surface forming a compact passive layer [34,35]. Further, due to the tendency of bond formation between the metal and the lone pair of electrons in the additive, the inhibition action is significantly enhanced [33]. The chemisorption of benzotriazole derivatives on the mild steel surface can take place based on donor–acceptor interactions between the p-electrons of the inhibitor and the vacant d-orbital of iron surface atoms [36]. The corrosion protection and release mechanism of benzotriazole has been shown schematically in Fig. 13. The grey part in the Fig. 13 is the weak section of the coatings where attack of corrosion species is significant, where the release of benzotriazole takes place in the presence of corrosion medium (pH 3, 5, 7 and 9). As discussed earlier, benzotriazole gives better corrosion inhibition in acidic and neutral medium and hence the release of benzotriazole has been tested under conditions of pH 3, 5, 7 and 9. The higher release of benzotriazole takes place at acidic pH value. The adsorption of benzotriazole molecule on the metal surface leads to a formation of the passive layer on the metal surface, which avoids the formation of corrosion cell; this in turn results into an enhancement in the corrosion resistance. The formed passive layer on MS panel inhibits the attack of corrosion species, which results in the improvement in the anticorrosion performance of $CaZn_2(PO_4)_2$ nanocontainer/alkyd coating.

4. Conclusions

The present study has successfully established a new approach for synthesis of $CaZn_2(PO_4)_2$ nanoparticles by ultrasound assisted chemical co-precipitation method and has also established that presence of ultrasonic irradiations can accelerate nucleation rate and result in good particle size distribution. The agglomeration of

$CaZn_2(PO_4)_2$ nanoparticles is substantially reduced due to ultrasonic irradiation resulting into nanometer sized calcium zinc phosphate nanoparticles with uniform distribution. Further, the present work confirmed the layer by layer assembly of $CaZn_2(PO_4)_2$ nanocontainers and the release mechanism of corrosion inhibitor. TEM and AFM study confirms the successful formation of $CaZn_2(PO_4)_2$ nanocontainer as a layer by layer system. Zeta potential and particle size analysis also shows the formation of layers and shows appropriate change in the surface charge, which could be responsible for the release mechanism initiated by the change in pH. Release study and corrosion results from Tafel plot and corrosion rate analysis showed significant improvement in the anticorrosion properties of coatings due to the optimum loading of the $CaZn_2(PO_4)_2$ nanocontainers.

Acknowledgments

S.H. Sonawane and A.B. Pandit acknowledge the support of Department of Science and Technology (DST), Government of India, for providing the Funds through Project Grant Reference No.: SR/S3/CE/0060/2010.

ReferenceS

[1] P. de Lima-Neto, A.P. de Araújo, W.S. Araújo, A.N. Correia, Study of the anticorrosive behaviour of epoxy binders containing non-toxic inorganic corrosion inhibitor pigments, Prog. Org. Coat. 62 (2008) 344–350.
[2] M.A. Abd El-Ghaffar, E.A.M. Youssef, N.M. Ahmed, High performance anticorrosive paint formulations based on phosphate pigments, Pigm. Resin Technol. 33 (2004) 226–237.
[3] B. Delamo, R. Romagnoli, V.F. Vetere, Steel corrosion protection by means of alkyd paints pigmented with calcium acid phosphate, Ind. Eng. Chem. Res. 38 (1999) 2310–2314.
[4] R. Zeng, Z. Lan, L. Kong, Y. Huang, H. Cui, Characterization of calcium-modified zinc phosphate conversion coatings and their influences on corrosion resistance of AZ31 alloy, Surf. Coat. Technol. 205 (2011) 3347–3355.
[5] K. Cheng, J. Zhou, W. Weng, S. Zhang, G. Shen, P. Du, G. Han, Composite calcium phosphate coatings with sustained Zn release, Thin Solid Films 519 (2011) 4647–4651.
[6] V. Palanivel, W.J. Van Ooij, Modified silane coatings as an alternative to chromates for corrosion protection of aluminum alloys, in: K.L. Mittal (Ed.), Silanes and Other Coupling Agents, vol. 3, Brill, 2004, pp. 135–159.
[7] I.M. Zin, S.B. Lyon, V.I. Pokhmurskii, Corrosion control of galvanized steel using a phospate/calcium ion inhibitor mixture, Corros. Sci. 45 (2003) 777–788.
[8] P.K. Sinha, R. Feser, Phosphate coating on steel surfaces by an electrochemical method, Surf. Coat. Technol. 161 (2002) 158–168.
[9] A. Valanezhad, K. Tsuru, M. Maruta, G. Kawachi, S. Matsuya, K. Ishikawa, Zinc phosphate coating on 316 L-type stainless steel using hydrothermal treatment, Surf. Coat. Technol. 205 (2010) 2538–2541.
[10] S. Ding, M. Wang, Studies on synthesis and mechanism of nano $CaZn_2(PO_4)_2$ by chemical precipitation, Dyes Pig. 76 (2008) 94–96.
[11] M.A. Patel, B.A. Bhanvase, S.H. Sonawane, Production of cerium zinc molybdate nano pigment by innovative ultrasound-assisted approach, Ultrason. Sonochem. 20 (2013) 906–913.
[12] S.H. Sonawane, S.R. Shirsath, P.K. Khanna, S. Pawar, C.M. Mahajan, V. Paithankar, V. Shinde, C.V. Kapadnis, An innovative method for effective micro-mixing of CO_2 gas during synthesis of nano-calcite crystal using sonochemical carbonization, Chem. Eng. J. 143 (2008) 308–313.
[13] P.R. Gogate, R.K. Tayal, A.B. Pandit, Cavitation: a technology on the horizon, Curr. Sci. 91 (2006) 35–46.
[14] A.V. Mahulkar, C. Riedel, P.R. Gogate, U. Neis, A.B. Pandit, Effect of dissolved gas on efficacy of sonochemical reactors for microbial cell disruption: experimental and numerical analysis, Ultrason. Sonochem. 16 (2009) 635–643.
[15] D.V. Pinjari, A.B. Pandit, Cavitation milling of natural cellulose to nanofibrils, Ultrason. Sonochem. 17 (2010) 845–852.
[16] S. Palraj, M. Selvaraj, P. Jayakrishnan, Effect of phosphate on the performance of epoxy polyamide red oxide primer on galvanized steel, Prog. Org. Coat. 54 (2005) 5–9.
[17] D.G. Shchukin, S.V. Lamaka, K.A. Yasakau, M.L. Zheludkevich, M.G.S. Ferreira, H. Mohwald, Active anticorrosion coatings with halloysite nanocontainers, J. Phys. Chem. C 112 (2008) 958–964.
[18] C. George, D. Dorfs, G. Bertoni, A. Falqui, A. Genovese, T. Pellegrino, A. Roig, A. Quarta, R. Comparelli, M.L. Curri, R. Cingolani, L. Manna, A cast-mold approach to iron oxide and Pt/iron oxide nanocontainers and nanoparticles with a reactive concave surface, J. Am. Chem. Soc. 133 (2011) 2205–2217.
[19] D.G. Shchukin, M. Zheludkevich, K. Yasakau, S. Lamaka, M.G.S. Ferreira, H. Mowald, Layer-by-layer assembled nanocontainers for self healing corrosion protection, Adv. Mater. 18 (2006) 1672–1678.
[20] I.A. Kartsonakis, G. Kordas, Synthesis and characterization of cerium molybdate nanocontainers and their inhibitor complexes, J. Am. Ceram. Soc. 93 (2009) 65–73.
[21] D.G. Shchukin, H. Möhwald, Surface-engineered nanocontainers for entrapment of corrosion inhibitors, Adv. Funct. Mater. 17 (2007) 1451–1458.
[22] Y.M. Abu, K. Aoki, Corrosion protection by polyaniline-coated latex microspheres, J. Electroanalyt. Chem. 583 (2005) 133–139.
[23] D.G. Shchukin, M. Zheludkevich, H. Möhwald, Feedback active coatings based on incorporated nanocontainers, J. Mater. Chem. 16 (2006) 4561–4566.
[24] B.A. Bhanvase, S.H. Sonawane, New approach for simultaneous enhancement of anticorrosive and mechanical properties of coatings: application of water repellent nano $CaCO_3$–PANI emulsion nanocomposite in alkyd resin, Chem. Eng. J. 156 (2010) 177–183.
[25] T.A. Kolesnikova, B.N. Khlebtsov, D.G. Shchukin, D.A. Gorin, Atomic force microscopy characterization of ultrasound-sensitive nanocomposite microcapsules, Nanotechnol. Russ. 3 (2008) 554–563.
[26] Y.B. Li, W.J. Weng, In vitro synthesis and characterization of amorphous calcium phosphates with various Ca/P atomic ratios, J. Mater. Sci.: Mater. Med. 18 (2007) 2303–2308.
[27] K.W. Wang, L.Z. Zhou, Y. Sun, G.J. Wu, H.C. Gu, Y.R. Duan, F. Chen, Y.J. Zhu, Calcium phosphate/PLGA-mPEG hybrid porous nanospheres: a promising vector with ultrahigh gene loading and transfection efficiency, J. Mater. Chem. 20 (2010) 1161–1166.
[28] O. Pawlig, R. Trettin, Synthesis and characterization of α-hopeite, $Zn_3(PO_4)_2{\cdot}4H_2O$, Mater. Res. Bull. 34 (1999) 1959–1966.
[29] Y. Sun, A.G. Macdiarmid, A.J. Epstein, Polyaniline: synthesis and characterization of pernigraniline base, J. Chem. Soc., Chem. Commun. 7 (1990) 529–531.
[30] M.M. Mennucci, E.P. Banczek, P.R.P. Rodrigues, I. Costa, Evaluation of benzotriazole as corrosion inhibitor for carbon steel in simulated pore solution, Cem. Concr. Compos. 31 (2009) 418–424.
[31] X. Lu, Y. Yu, L. Chen, H. Mao, L. Wang, W. Zhang, Y. Wei, Poly(acrylic acid)-guided synthesis of helical polyaniline microwires, Polymer 46 (2005) 5329–5333.
[32] P. Matheswaran, A.K. Ramasamy, Influence of benzotriazole on corrosion inhibition of mild steel in citric acid medium, E.-J. Chem. 7 (2010) 1090–1094.
[33] S.T. Selvi, V. Raman, N. Rajendran, Corrosion inhibition of mild steel by benzotriazole derivatives in acidic medium, J. Appl. Electrochem. 33 (2003) 1175–1182.
[34] A. Popova, M. Christov, Evaluation of impedance measurements on mild steel corrosion in acid media in the presence of heterocyclic compounds, Corros. Sci. 48 (2006) 3208–3221.
[35] P.G. Cao, J.L. Yao, J.W. Zheng, R.A. Gu, Z.Q. Tian, Comparative study of inhibition effects of benzotriazole for metals in neutral solutions as observed with surface enhanced Raman spectroscopy, Langmuir 18 (2002) 100–104.
[36] S. Ramesh, S. Rajeswari, Corrosion inhibition of mild steel in neutral aqueous solution by new triazole derivatives, Electrochim. Acta 49 (2004) 811–820.
[37] T. Murakawa, S. Nagaura, N. Hackerman, Coverage of iron surface by organic compounds and anions in acid solutions, Corros. Sci. 7 (1967) 79–89.